Nuclear Instruments and Methods in Physics Research A285 (1989) 128–131
North-Holland, Amsterdam

INTERPRETATION OF WAVE-PROFILE MODIFICATION MEASUREMENTS IN HIGH-GAIN RAMAN FREE-ELECTRON-LASER EXPERIMENTS

E. JERBY and A. GOVER

Faculty of Engineering, Tel Aviv University, Tel Aviv, Israel 69978

This paper presents a theoretical analysis of wave-profile modification measurements in FELs, using data that was reported recently [Phys. Rev. Lett. 59 (1987) 1177]. The results are related to a high-gain Raman free-electron laser, operating at long wavelengths (~ 3 cm). Two possible mechanisms for wave-profile modification were examined. One is the known e-beam optical guiding effect. The other is that of the transverse electrostatic fields (TEF), excited by the bunched electron beam. The numerical results suggest that in the above-mentioned reference the measured wave-profile modification was predominantly a consequence of the TEF components. An experimental setup for verification of this analysis is proposed.

1. Introduction

Effects of wave-profile modification due to FEL interaction are of great importance in understanding the FEL physics and in the design of new FELs. The optical guiding effect [2] in high-gain FELs produces confinement of the EM wave profile near the e-beam and consequently a higher gain. Another transverse-field effect is the creation of transverse electrostatic fields (TEF) by the bunched electron beam due to its finite transverse dimensions [3,4,6]. In FELs it may modify the synchronism condition and the gain with respect to the 1D-model predictions. These two effects, optical guiding and TEF, may occur simultaneously. Although they are consequences of different mechanisms, they have similar profile shapes outside the electron beam. Therefore, a clear distinction between them is called for in theory and experiments.

Measurements of wave-profile modification in a high-gain free electron laser were published recently [1].

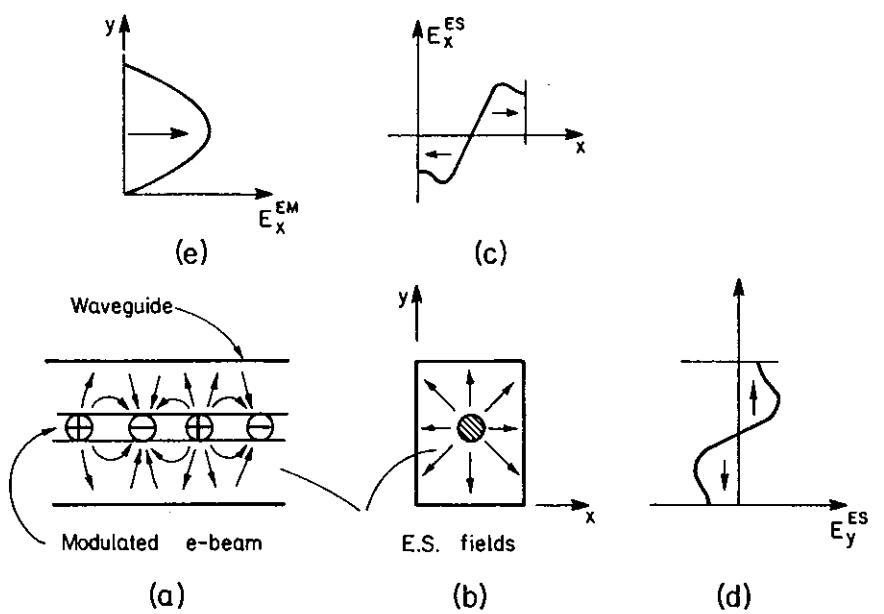

Fig. 1. A figurative description of the electrostatic wave components, spread out of a bunched e-beam in a waveguide: the longitudinal (a) and transverse (b) cross section in the waveguide, the x-polarized (c) and the y-polarized (d) electrostatic wave components, and the TE_{10} waveguide mode profile (e).

0168-9002/89/$03.50

This FEL was operating at a long wavelength (~ 3 cm) in the Raman regime. The reported wave profiles are concentrated in the vicinity of the e-beam cross section. This kind of shape may be anticipated when the optical-guiding mechanism exists in high-gain FELs. However, such profile modification effects can also be produced by other physical mechanisms such as the TEF, and particularly by a 3-D space-charge wave interference effect to be discussed henceforth.

A three-dimensional theoretical FEL model [3] and a numerical analysis were applied to analyze the result of ref. [1] in order to determine what was the main physical effect responsible for the measured wave-profile modification. The theoretical analysis shows that the modification in the electric-field profile may be attributed to interference of (slow) electrostatic fields and the amplified fundamental TE_{10} mode. The optical-guiding effect was found negligible in this case. The electrostatic fields, which in a transversely infinite system (1D limit) are considered to be purely axial, have significant transverse components in a finite-beam cross-section case (3D model). The transverse components of the electrostatic fields fringe out of the bunched e-beam toward the waveguide walls, as shown in fig. 1. This effect is also known as the cause for the reduction of the effective plasma frequency in bound-electron beams [4].

2. Theoretical model and numerical results

The profile of the amplified electromagnetic wave (at the exit of the FEL) was computed by solving the 3D gain-dispersion matrix equation

$$\boldsymbol{E}_X^{(0)} = \left\{ \left[\mathbf{I} + \mathbf{R}\chi_z^{(+1)} \right] \mathbf{K}^{(0)} - \mathrm{i}\kappa \mathbf{G}\chi_z^{(+1)} \right\}^{-1} \times \left[\mathbf{I} + \mathbf{R}\chi_z^{(+1)} \right] \hat{\boldsymbol{E}}_{X0}. \quad (1)$$

This 3D equation was presented and explained in refs. [3,5–7]. The EM field vectors, $\boldsymbol{E}_X^{(0)}$ and $\hat{\boldsymbol{E}}_{X0}$, consist of vector components, each of which represents a discrete transverse spatial Fourier component of the radiation wave, where $\hat{\boldsymbol{E}}_{X0}$ corresponds to the entrance to the interaction region and $\boldsymbol{E}_X^{(0)}$ is the Laplace transform (in the z-dimension) of the spatial Fourier components at the exit. This representation can be regarded as an expansion of the field in terms of a spectrum of plane waves. Waveguide modes are represented in this formulation by a linear combination of two or four plane waves. The unit matrix is denoted $\mathbf{I}$, and $\mathbf{R}$ is the space-charge reduction matrix. $\mathbf{K}^{(0)}$ is a diagonal matrix that represents the EM-wave-propagation constants of the various plane waves (spatial Fourier components). The matrix $\mathbf{G}$ is the e-beam coupling matrix. It consists of the transverse spatial Fourier components of the e-beam profile function $g(x, y)$ which are packed in the matrix in a way which performs a numerical convolution operation between the spatial Fourier spectra of the e-beam and the radiation beam profiles. The coupling parameter is κ, and $\chi_z^{(+1)}$ is the 1D longitudinal susceptibility of the bunched electron beam [8]. The space-charge reduction matrix $\mathbf{R}$ was found to be [3]

$$\mathbf{R} = -\frac{\omega^2}{2\langle \gamma_z^2 v_z^2 \rangle (s + \mathrm{i}k_W)} \mathbf{G} (\mathbf{K}^{(+1)})^{-1}. \quad (2)$$

The indices (0, +1) correspond to various Floquet space harmonics, Thus $\mathbf{K}^{(+1)}$ is equal to $\boldsymbol{K}^{(0)}$ shifted by the transformation $s \to s + \mathrm{i}k_W$ in the complex s-plane (s is the Laplace transform variable corresponding to z).

The profiles of the electrostatic waves were computed by solving another 3D dispersion equation [3,6]:

$$\boldsymbol{E}_Z^{(+1)} = \frac{\mathrm{i}sV_{Wx}}{2\omega} \mathbf{R}' \chi_z^{(+1)} \left[\mathbf{K}^{(0)} \left[\mathbf{I} + \mathbf{R}' \chi_z^{(+1)} \right] - \mathrm{i}\kappa \mathbf{G} \chi_z^{(+1)} \right]^{-1} \hat{\boldsymbol{E}}_{X0}. \quad (3)$$

This equation describes the relation between the longitudinal component of the slow (order +1) Floquet component which is the electrostatic (ES) wave $\boldsymbol{E}_Z^{(+1)}$ and the initial electromagnetic (EM) wave at the entrance, $\hat{\boldsymbol{E}}_{X0}$. The ES waves are distinguished here from the EM waves by their phase velocity, which is close to the e-beam velocity ($v_z \sim \omega/[\mathrm{Re}\{s\} + k_W]$). The transverse components of the ES wave are related to its longitudinal component by [3,6]

$$\boldsymbol{E}_X^{(+1)} = \gamma_z^2 \langle \bar{v}_z \rangle \frac{k_{0x}}{\omega} \mathbf{N} \boldsymbol{E}_Z^{(+1)}, \quad (4)$$

where the vector $\boldsymbol{E}_Z^{(+1)}$ is found from eq. (3). The reduction matrix for the electrostatic waves, $\mathbf{R}'$, is given by

$$\mathbf{R}' = -\frac{\omega^2}{2\langle \gamma_z^2 \bar{v}_z^2 \rangle (s + \mathrm{i}k_W)} (\mathbf{K}^{(+1)})^{-1} \mathbf{G}. \quad (5)$$

It is noted that $\mathbf{R}'$ differs from $\mathbf{R}$ [eq. (2)] by the reversed order of the matrix multiplication, $(\mathbf{K}^{(+1)})^{-1}\mathbf{G}$. The gain dispersion equation for $\boldsymbol{E}_Z^{(+1)}$ [eq. (3)] differs from the one for $\boldsymbol{E}_X^{(0)}$ [eq. (1)] by the position of the wavenumber matrix $\mathbf{K}^{(0)}$ in its denominator. Therefore its poles and zeros in the s-plane are not the same as those of eq. (1).

Eqs. (1), (3) and (4) were used to calculate the profiles of the EM and ES waves according to the parameters of ref. [1], at $L_W = 1.32$ m (40 wiggles). Fig. 2 shows the computed amplitude profiles of the input and the output EM waves, and the e-beam current-density profile, which is in this case taken to have a Gaussian shape. The profile of the amplified output wave looks similar to that of the fundamental TE_{10} mode, which is the input field. No observable profile modification is seen in this component, which is the solenoidal radiation field. This is a reasonable result,

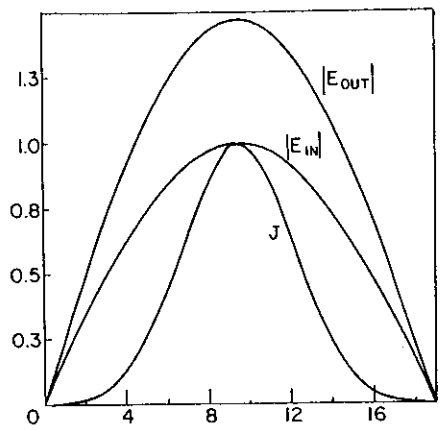

Fig. 2. The amplitude profiles of the electromagnetic waves at the entrance and the exit of the interaction region for the MIT [1] FEL parameters. J is the current density profile.

taking into account that the next waveguide mode (the TE_{20} or the TE_{01}) is in cutoff and is decaying at a rate of 248 m^{-1}.

The profiles of the ES waves in the $\hat{x}$- and $\hat{y}$-directions are shown in figs. 3a and b, respectively. These computed profiles of E_z, E_x and E_y have similar shapes to the profiles sketched in fig. 1. Examination of the ES wave profile curves (fig. 3) indicates that the transverse field components are not negligible, and are even greater than the axial components of the ES wave. Note that the displayed profiles correspond to the absolute values of the fields. The phase profiles were also calculated but are not shown here. The transverse electrostatic field components, $\mathrm{Re}\{E_x^{ES}(x, y)\}$ and $\mathrm{Re}\{E_y^{ES}(x, y)\}$, are essentially the fringe fields of the beam space-charge bunches and therefore are antisymmetric and vanish on axis. The longitudinal field $E_x^{ES}(x, y)$ is symmetric.

3. Interference of EM waves and ES waves

In order to interpret the result reported in ref. [1], we propose that the measured profiles (fig. 4 in ref. [1]) correspond to probe measurements of the product of two field signals, the electromagnetic wave E_x^{EM} and the electrostatic wave E_x^{ES}. The power $P(x, y)$ measured by the probe is relative to the square of the total field amplitude, $|E_x^{EM} + E_x^{ES}|^2$. The probe measures the intensity in both equal frequency fields $|E_x^{EM}|^2$ and $|E_x^{ES}|^2$, but also measures a superimposed interference term $2\mathrm{Re}\{E_x^{EM}E_x^{ES*}\}$. Even when $|E_x^{ES}| \ll |E_x^{EM}|$, this interference term can produce a significant contribution. The computed amplitude of E_x^{EM} is about 1.45 and the extremum values of E_x^{ES} are ± 0.04. Hence one may expect a power intensity variation across the beam in the $\hat{x}$ (narrow) dimension of the WG of more than 10%, superimposed on the power profile of the radiation mode $|E_x^{EM}|^2$. In the case that the e-beam profile was assumed as a cylinder with sharp edges, the field E_x^{ES} reaches ± 0.07 and the power-intensity transverse variation is almost doubled.

4. Notes on experimental methods

Although the interpretation given here for the wave-profile modification measurements [1] provides a reasonable explanation for the reported results, there still is a considerable difference between the measured and the calculated results. The quantitative difference can be explained by various reasons. Due to the experimental limitation, the probe used in the experiment could peak up an additional in-phase component of E_y^{ES} and further increase the difference. A second reason can be associated with the lack of transparancy of the probe mounting, which could produce a non-negligible profile

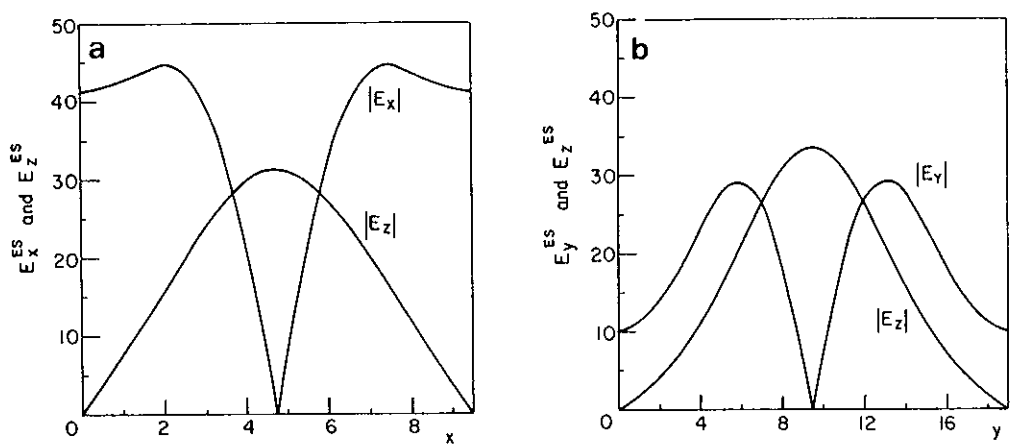

Fig. 3. The relative amplitudes of the electrostatic wave components in the x-direction (a), the y-direction (b) and the z-direction (a and b), given in per mills of the input EM amplitude in fig. 2.

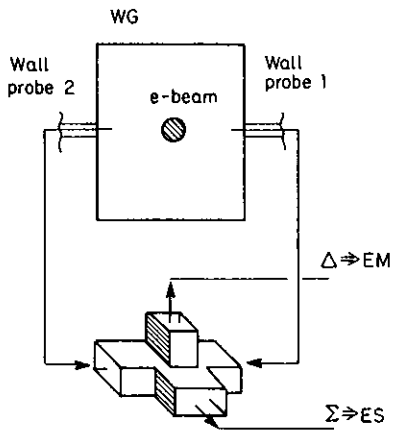

Fig. 4. Experimental setup for separating electromagnetic and electrostatic wave components on the waveguide walls. The signals received by a pair of nonpenetrating probes are summed and subtracted by a magic-T waveguide junction.

modification effect on the electrostatic field profile. Yet another reason for the quantitative difference is that we did not take into account here the transverse scanning of the electron beam across the WG cross section that was implemented in the experiment, but rather calculated the profile of the fields for an axially centered electron beam.

To achieve a better quantitative fit between the experimental and the theoretical results, it is proposed to use a nonpenetrating probe measurement, using a similar setup as that shown in ref. [1]. This can be accomplished by installing an additional (nonpenetrating) wall probe on the other waveguide wall (in the same cross section). The outputs of both probes can be summed and subtracted (in rf) by a magic-T waveguide junction, as shown in schematically fig. 4. This may provide means to distinguish between the EM and ES wave components, taking advantage of their opposing symmetry and anti-symmetry features. In this way one may distinguish between the perpendicular components of the electromagnetic waves and the electrostatic waves on the walls. Knowing the bunching wavenumber $\omega/\bar{v}_z$ and assuming a relatively narrow e-beam profile one can compute the entire profile of the transverse ES waves from their value on the walls.

Acknowledgements

The authors acknowledge communications with G. Bekefi and J. Wurtele. This work was supported in part by the US ONR under contract no. N00014-87-C0362.

References

[1] F. Hartemann, K. Xu, G. Bekefi, J.S. wurtele and J. Fajans, Phys. Rev. Lett. 59 (1987) 1177.
[2] E.T. Scharlemann, A.M. Sessler and J.M. Wurtele, Phys. Rev. Lett. 54 (1985) 1925.
[3] E. Jerby, Ph.D. thesis, Tel Aviv University, 1988.
[4] G.M. Branch and T.G. Mihra, IEEE Trans. Electron Devices ED-2 (1955) 3.
[5] E. Jerby and A. Gover, Nucl. Instr. and Meth. A272 (1988) 380.
[6] E. Jerby and A. Gover, Phys. Rev. Lett. 63 (1989) 864.
[7] R.W. Best et al., these proceedings (10th Int. Free Electron Laser Conf., Jerusalem, 1988) Nucl. Instr. and Meth. A285 (1989) 211.
[8] E. Jerby, Nucl. Instr. and Meth. A272 (1988) 457.